IEEE Photonics Journal
An IEEE Photonics Society Publication

Open Access

Faster and More Accurate Time Domain Electromagnetic Simulation Using Space Transformation

Volume 12, Number 4, August 2020

Mohammadrahim Kazemzadeh
Weiliang Xu
Neil G.R. Broderick

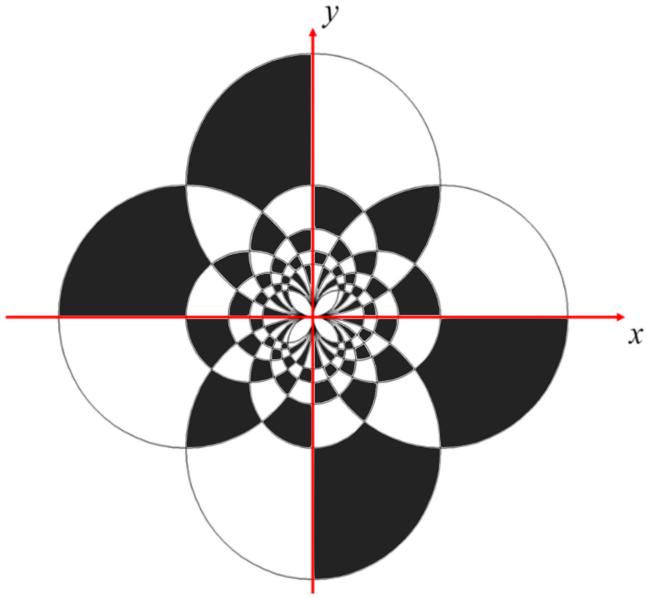

DOI: 10.1109/JPHOT.2020.3005704

IEEE photonics SOCIETY
IEEE

Faster and More Accurate Time Domain Electromagnetic Simulation Using Space Transformation

Mohammadrahim Kazemzadeh,[1] **Weiliang Xu**,[1] **and Neil G.R. Broderick**[2]

[1]Department of Mechanical Engineering, The University of Auckland, Auckland 1010, New Zealand
[2]Department of Physics, The University of Auckland, Auckland 1010, New Zealand

DOI:10.1109/JPHOT.2020.3005704

Manuscript received May 11, 2020; revised June 20, 2020; accepted June 25, 2020. Date of publication June 29, 2020; date of current version July 14, 2020. Corresponding author: Mohammadrahim Kazemzadeh (e-mail: mkaz499@aucklanduni.ac.nz).

Abstract: A novel finite difference time domain (FDTD) method based on space transformations is developed that overcomes the inherent obstacles of the conventional FDTD algorithm in a spatially complex domain. Our method leads to an adaptive mesh for the investigated structure based on its geometrical shape without adding additional numerical problems such as late-time instability. In this method, mesh boundaries can follow arbitrary geometrical shapes precisely meaning that discretization errors are minimized. Such errors can be considerable when dealing with large material differences or boundary conditions within the simulation domain. Different meshing and transformation techniques for a variety of different scenarios are presented. We show how boundaries discontinuity can be handled using our method without resulting artificial singularities or zeros. Unlike previous works no dispersive medium has been used so the simulation speed is similar to the standard FDTD method. The usability and superiority of this method in terms of simulation run time and accuracy are shown through a couple of scattering and plasmonic problems. Also, the result of any simulations are validated using finite element method.

Index Terms: Transformation optics, plasmonic, waveguide, FDTD, SERS.

1. Introduction

Plasmonic surfaces have found applications in many areas of science such as effective energy harvesting devices [1]–[2], biomedical applications [3], [4] and even second or third harmonic generation [5], [6]. Surface-enhanced Raman scattering (SERS) [7] also benefits from plasmonic effects thanks to the huge nonlinear enhancement of the electric field. Practically, SERS can enhance the Raman signal by up to a factor of 10^6 since the strength of the Raman signal is proportional to fourth power of the amplitude of the local electric field which is itself dramatically increased near a plasmonic resonance [8]. In order to fully exploit the SERS effect, we need to use computational electromagnetics to design, optimize and investigate possible plasmonic structures. However, as sharp edges and nanometer size separations between nanoparticles are required for huge electric field enhancement [9], sophisticated adaptive meshing technique requiring large computational resources are typically needed to accurately model such devices.

In the literature [10]–[12], two main numerical methods have been applied to investigate plasmonic structures, i.e. the finite element method (FEM) and the finite difference time-domain (FDTD)

method. For many optical applications, FDTD is preferred since it directly allows us to investigate the nonlinear behavior of materials and obtain their frequency responses by performing a single simulation. However, when the problem contains sub-wavelength geometrical details [13] across a relatively large computational domain it is very difficult to obtain accurate results by FDTD. Sub-gridding FDTD algorithms are one of the most popular approaches that can help to overcome this problem [14], [15]. In spite of its accuracy, the sub-gridding technique mostly suffers from late-time simulation instability, especially when a relatively high gridding ratio is chosen. As the huge Raman scattering enhancement can only be achieved through sharp and subwavelength variation of geometry, all the previously mentioned problems are inevitable.

In a series of papers [16]–[20] researchers have tried to find an analytical solution for plasmonic wave propagation around geometrical singularities potentially solving these issues. They used transformation optics [21] to find two equivalent physical scenarios one with a geometrical singularity at the origin and the other one with a uniform geometry but with mapped singularities at infinity. Next the problem for the uniform geometry, (e.g. a uniform metal insulator metal (MIM)) structure is solved analytically then this solution is transformed back into the original space. Although this method provides us with an insightful way to investigate the local plasmonic mode around geometrical singularities, it involves a lot of assumptions resulting in various limitations. For example, mapping an infinite space, with a singularity at infinity, to a finite one the material parameters around the origin singularity will also become singular. It can be avoided by including a limitation on the lengths of uniform structures so that in the transformed space material parameters remain non-singular.

Another major limitation is related to the size of the investigated structures. Using a conformal transformation approach results in a modified permittivity and permeability distribution in the transformed space [22]. This modified material distribution becomes important when modelling structures with a diameter smaller than 200 nm [16] and with sharp edges in sub-nanometer sizes (for optical wavelengths). Such geometries are not only feasible using current fabrication techniques but also essential for many existing SERS designs. For instance Refs [12] & [23] demonstrate that Raman scattering amplification of more than million have been achieved with geometric features around a few microns.

In addition, recent research has brought the notion of transformation optics into the area of numerical analysis. In [13], [24]–[27] the simulation geometry was transformed so that more meshing cells were placed on a small object by enlarging the area around it. Ref [13] showed that transformation optics FDTD is superior in terms of stability and accuracy in comparison to sub-gridding FDTD. However, all these methods still suffer from discretization errors as the cubic grid of FDTD points cannot easily follow curved boundaries. Another problem of all these methods is that they use dispersive media to model the transformed materials with relative permittivity and permeability smaller than unity. This dispersive medium adds unwanted frequency dependency to the simulation which tightly constrains the useful frequency bandwidth of the simulation.

In this research, we focus on combining the two previously mentioned numerical and analytical techniques, to compensate for their individual disadvantages. Firstly, different mapping techniques are investigated to demonstrate their advantages and disadvantages and then the mathematical reasons for the presence of material singularity in transformed space are found and compensated for using a novel transformation. Additionally, the effect of mapping on the meshing scheme is shown. We show how improved mapping can avoid the discretization error in the FDTD algorithm. Also, it is shown that the proposed mapping can automatically generate an adaptive mesh in the transformed space. Furthermore, a reverse technique is proposed to obtain the transformation parameters from the meshed structure. It is shown that this technique can compensate some of the old obstacles in the FDTD algorithm. Finally, a novel technique is proposed to handle numerical instability caused by small predicted permittivity and permeability while we have control over the simulation time step.

The superiority of the proposed technique is shown through a couple of examples of SERS and MIM structures. Also, the simulation results have been validated by comparing the results from the conventional FDTD and FEM numerical methods.

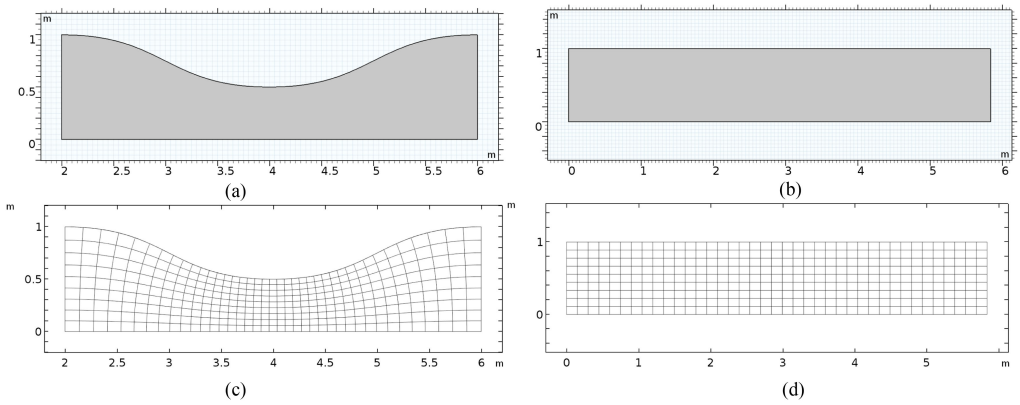

Fig. 1. (a) and (b) physical and virtual space geometry, respectively. (c) and (d) coordinate grid in virtual space and its distribution in physical space.

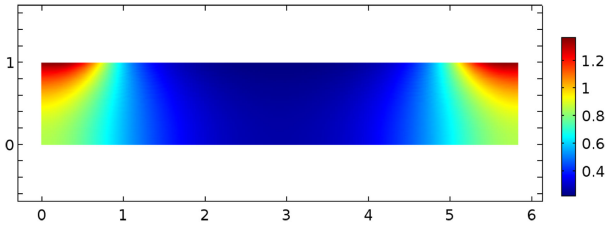

Fig. 2. Distribution of ε_{zz} in geometry of Fig. 1(b) using conformal transformation.

2. Methodology

The goal of transformational optics is to create two equivalent optical systems, with two different geometries and different material parameters which are related by a specified diffeomorphism. This allows us to alter the geometry of our initial problem to make it easier to be solved either numerically [13], [24]–[27] or analytically [16]–[20]. For instance, consider the non-uniform structure which is illustrated in Fig. 1(a). Suppose that we illuminate the left-hand end and want to know how much light is reflected or transmitted. Solving this problem analytically or using a FDTD calculation is a very hard task as the domain of interest has a curved boundary. But if we transform this geometry to Fig. 1(b) the problem becomes easier to be handled as all the boundaries are uniform. Now consider a general diffeomorphism $\mathbf{T}$ that maps $\mathbf{R^3}$ to $\mathbf{R^3}$. This transformation and its inverse can be expressed as follows:

$$\begin{aligned} \mathbf{x}' &= \mathbf{T}(\mathbf{x}) \\ \mathbf{x} &= \mathbf{T}^{-1}(\mathbf{x}') \end{aligned} \tag{1}$$

where $\mathbf{x}$ and $\mathbf{x}'$ are arbitrary points in physical space and virtual space, respectively. Note that locally the transformation is approximated by:

$$\mathbf{x}'_0 + \Delta\mathbf{x}' = \mathbf{T}(\mathbf{x}_0 + \Delta\mathbf{x}) \approx \mathbf{T}(\mathbf{x}_0) + \mathbf{\Lambda}\Delta\mathbf{x} \tag{2}$$

where $\mathbf{\Lambda}$ is the Jacobean of the transformation. For the virtual space to be equivalent physically to the real space the material parameters in each space must be related by [21]:

$$\begin{aligned} \varepsilon' &= \frac{\mathbf{\Lambda}\varepsilon\mathbf{\Lambda}^T}{\det(\mathbf{\Lambda})} \\ \mu' &= \frac{\mathbf{\Lambda}\mu\mathbf{\Lambda}^T}{\det(\mathbf{\Lambda})} \end{aligned} \tag{3}$$

Fig. 3. (a) Boundary discontinuity in physical space. (b) continuous boundary in virtual space.

where ε, ε',μ and μ' are permittivity, permeability in physical and virtual spaces respectively and det($\mathbf{\Lambda}$)denotes the determinant of the Jacobean. Similarly, the electric and magnetic fields in physical and virtual space obey:

$$\mathbf{E}' = \mathbf{\Lambda}^T \mathbf{E}$$
$$\mathbf{H}' = \mathbf{\Lambda}^T \mathbf{H} \tag{4}$$

where **E**, **E**′, **H** and **H**′ represent the electric and magnetic fields in the physical and virtual spaces.

Using Eqs. (1)–(4), we can transform our problem with its subwavelength geometrical variations into a virtual space that is spatially uniform but with varying material parameters making it significantly easier to solve numerically. Then, after finding the field distribution in virtual space, e.g. using conventional FDTD, we can apply the reverse transformation in order to find the electric and magnetic fields in physical space.

As a starting point we consider conformal transformations since both the transformation and its inverse are then smooth and infinitely differentiable. For the example in Fig. 1, we can solve Laplace's equation to find the appropriate transformation to go from real space, Fig. 1(a), to virtual space, Fig. 1(b), and back again. The virtual space grids and its transformed grid in physical space are shown in Fig. 1(d) and (c) respectively. Actually, these grids represent the schematic of the FDTD meshing scheme in both spaces. As the conformal transformation preserves angles, we can see the mapped grids in physical space, Fig. 1(c), are still locally perpendicular. One of the challenges in the way of using conformal transformation is the presence of singularity [22] in the calculated materials.

2.1 Effects of Transformation on Material Singularities And Zeros

One of the major challenges in this approach lies in the presence of singularities in the new material parameters. To have an accurate simulation, we should place a number of meshes points in each area inversely proportional to the local wavelength. In places with high relative permittivity and permeability, the wavelength tends to zero and the number of mesh points tends to infinity. Hence an accurate simulation in the presence of a material singularity is almost impossible. Such singularities can arise in the transformed space due to the presence of geometric discontinuities in real space (i.e. corners). Consider the scenario which is depicted in Fig. 3. If we rewrite Eq. (2) for the two given vectors which are infinitely close to the boundary discontinuity. We will have the following equation [28],

$$\begin{bmatrix} \Lambda_{xx} & \Lambda_{xy} \\ \Lambda_{yx} & \Lambda_{yy} \end{bmatrix} \begin{bmatrix} P_{1x} & P_{2x} \\ P_{1y} & P_{2y} \end{bmatrix} = \begin{bmatrix} P'_{1x} & P'_{2x} \\ P'_{1y} & P'_{2y} \end{bmatrix} \tag{5}$$

in which P_{iq} and P'_{iq} $i = \{1, 2\}$ and $q = \{x, y, z\}$ represent the components of each vectors in physical and virtual space, respectively. Now if we take determinant from two sides of Eq. (5) we will have

$$\det\left(\begin{bmatrix} \Lambda_{xx} & \Lambda_{xy} \\ \Lambda_{yx} & \Lambda_{yy} \end{bmatrix}\right) \text{ (area between vectors } \mathbf{p}_1 \text{ and } \mathbf{p}_2) = \text{(area between vectors } \mathbf{p}'_1 \text{ and } \mathbf{p}'_2) \tag{6}$$

Note that the area between $\mathbf{p}'_1$ and $\mathbf{p}'_2$ is zero while the area between $\mathbf{p}_1$ and $\mathbf{p}_2$ is non zero. This forces the determinant of the left-hand side matrix, which is the Jacobean matrix of transformation,

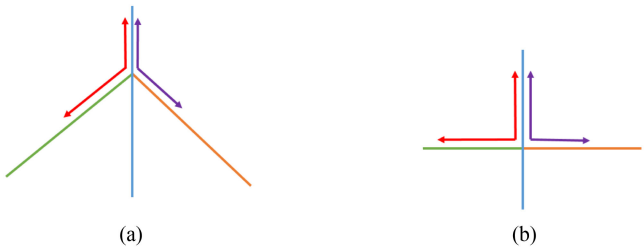

Fig. 4. Blue partition lines create two subspace in which the transformed material cannot become singular. (a) physical space. (b) virtual space.

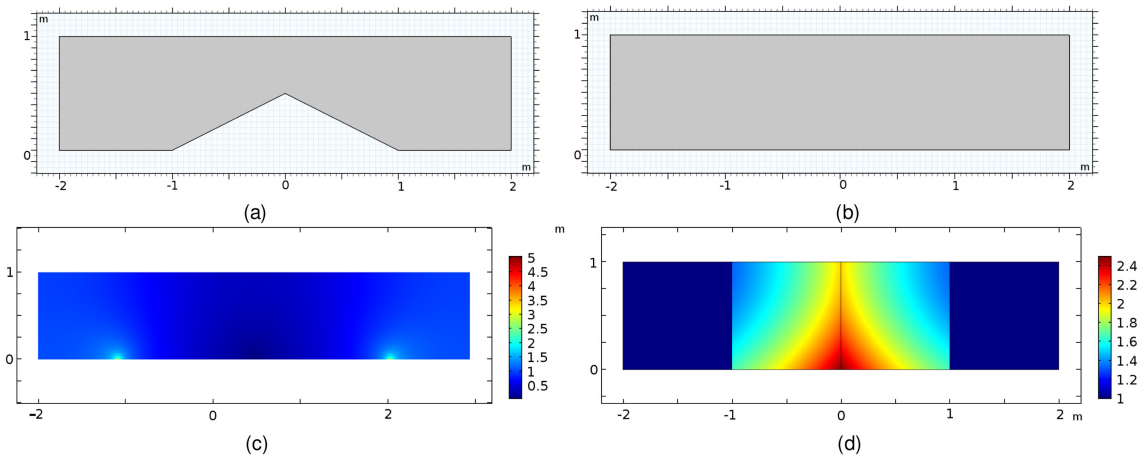

Fig. 5. (a) and (b) physical and virtual space geometry. (c) calculated ε_{zz} distribution using conformal transformation. (d) distribution of ε_{zz} using discontinuous mapping.

to be zero. According to Eq. (3), if the determinant of the Jacobian matrix of transformation is zero the transformed material will become singular. If we consider the reverse scenario, mapping a flat boundary to discontinuous one, we will have an infinity for the determinant of the Jacobian matrix which will lead to a zero in the material property.

This singularity and zero can easily be avoided by creating a section at discontinuity as it is shown in Fig. 4. Each side of this section must be mapped according to its specific transformation. Now, Eq. (5) is no longer valid since two different transformations are used for the two vectors $\mathbf{P_1}$ and $\mathbf{P_2}$. It can be concluded in this way that if we have a discontinuity on a boundary, we need to divide the geometry into discrete sections to ensure that there is no boundary discontinuity in each section. Therefore, the discontinuity at the boundary will lead to the discontinuity at the mapping instead of a material singularity or zero.

The usefulness of the above procedure is shown in Fig. 5. Physical space geometry with three discontinuity at its boundary and uniform virtual space geometries are shown in Fig. 5(a) and (b), respectively. The predicted material for the virtual space using the conformal transformation is shown in Fig. 5(c). As it is shown it has two singularities and one zero. This happened while neither singularity nor zero is presented when we map each section independently, Fig. 5(d). The general formulas for the transformation, of discontinuous areas are given by

$$y' = -a\frac{a-y}{a-f(x)} + a$$
$$x' = g(x) \tag{7}$$

in which x, y, x' and y' are the coordinate of physical and virtual spaces, respectively and f(x), g(x) and "a" denote the geometrical mapping functions between discontinuities. Note that we can have different x-direction meshing distribution by changing g(x). For example, if we choose g(x) to be 2x we have 2 times more uniform meshes along x-direction in the transformed area. For the result of the left side discontinuity of Fig. 5(d) we have chosen the "a", f(x) and g(x) to be 2, x/2 + 1 and x, respectively.

The only drawback of this approach is that the transformed material becomes anisotropic since we did not use a conformal transformation as can be seen in Fig. 5(d).

2.2 CFL Numerical Stability Condition

From Eq. (3) and Fig. 5 it can be seen that in some areas the transformed relative permittivity and permeability become smaller than one. These reductions are very problematic in an explicit FDTD algorithm since the grid must be sub-wavelength and the time step sufficiently small to stop numerical instabilities (i.e. the Courant–Friedrichs–Lewy (CFL) condition). Simply decreasing the time step can solve this problem but at the expense of making the simulations extensively time consuming. Thus, below we discuss a number of ways around this issue.

One of the ways to solve this problem is by using dispersive materials [24]–[27]. However, there are two major constraints on the definition of dispersive materials before they are suitable for inclusion in an explicit FDTD simulation. The first one is that the material must not make the simulation unstable. Mathematically, this means that all the poles of the transfer function of the proposed dispersive material must be on the left-hand side of the complex plane. The second one is, the material must not be lossy if there is no source of loss in physical space. The last constraint limits the poles lie on the imaginary axis. As a result, the general form of the dispersive materials must be

$$H(s) = \sum_n \frac{A_n}{{\omega_n}^2 + s^2}$$
$$H(j\omega) = \sum_n \frac{A_n}{{\omega_n}^2 - \omega^2} \tag{8}$$

in which H, A_n, ω_n, s and ω are the transfer function, constant numbers and real numbers, complex and real angular speed, respectively. It is clear that the above dispersion formulas are just the Drude model for a lossless medium. Although such a material will make the simulation stable, it limits the bandwidth of the simulation [13], [24]–[26]. This constraint should not be considered as an obstacle when simulating many potential SERS devices as the excitation in Raman spectroscopy is done using a monochrome laser with a very short bandwidth. But however, this constraint can cause problems when dealing with the propagation of short pulses or broadband width plasmonic devices.

Instead we propose another method using a transformation suitable for FDTD simulations involving materials with refractive indices less than one. We start with the observation that for a lossless material the transformed permittivity and permeability tensors are Hermitian and so can be diagonalized using a proper rotation. Therefore, for each mesh, cell we can write the general material properties in an orthonormal coordinate system as

$$\varepsilon'^{\mathbf{R}} = \begin{bmatrix} {\varepsilon'_{xx}}^R & 0 & 0 \\ 0 & {\varepsilon'_{yy}}^R & 0 \\ 0 & 0 & {\varepsilon'_{zz}}^R \end{bmatrix}$$
$$\mu'^{\mathbf{R}} = \begin{bmatrix} {\mu'_{xx}}^R & 0 & 0 \\ 0 & {\mu'_{yy}}^R & 0 \\ 0 & 0 & {\mu'_{zz}}^R \end{bmatrix} \tag{9}$$

in which $\varepsilon'^{\mathbf{R}}$and $\mu'^{\mathbf{R}}$ are the permittivity and permeability tensors in the new rotated orthonormal coordinate system. Now, consider making an anisotropic coordinate expansion transformation given by a matrix **m.** By Eq. (3) it results in a new permeability tensor given by:

$$\mathbf{m} = \begin{bmatrix} m_x & 0 & 0 \\ 0 & m_y & 0 \\ 0 & 0 & m_z \end{bmatrix}$$

$$\varepsilon'^{\mathbf{R}}_{\mathbf{new}} = \begin{bmatrix} \varepsilon'^{R}_{xx} \frac{m_x^2}{m_x m_y m_z} & 0 & 0 \\ 0 & \varepsilon'^{R}_{yy} \frac{m_y^2}{m_x m_y m_z} & 0 \\ 0 & 0 & \varepsilon'^{R}_{zz} \frac{m_z^2}{m_x m_y m_z} \end{bmatrix} \tag{10}$$

in which m_x, m_y and m_z are the amount of coordinate expansion in each direction. Crucially this gives us independent control over each component of permeability tensor. Thus, we can apply a unique anisotropic expansion over the whole geometry to ensure that material's refractive index is always greater than unity.

Let's make it clear by an example of conformal transformation. The general material property resulting from the conformal transformation can be expressed as

$$\varepsilon' = \begin{bmatrix} 1 & 0 & 0 \\ 0 & 1 & 0 \\ 0 & 0 & f(i,\, j) \end{bmatrix} \tag{11}$$

in which the $f(i, j)$ is the value in *(i, j)* meshing cell. Now we apply the anisotropic coordinate expansion

$$\mathbf{m} = \begin{bmatrix} \sqrt{\min(f(i,\, j))} & 0 & 0 \\ 0 & \sqrt{\min(f(i,\, j))} & 0 \\ 0 & 0 & 1 \end{bmatrix} \tag{12}$$

$$\varepsilon'_{\mathbf{new}} = \begin{bmatrix} 1 & 0 & 0 \\ 0 & 1 & 0 \\ 0 & 0 & \frac{f(i,j)}{\min(f(i,j))} \end{bmatrix} \tag{13}$$

in which $\min(f(i, j))$ is the minimum of$f(i, j)$ in the computational domain. As we can see from Eq. (13) the material's refractive index is >1 everywhere in the transformed domain. This transformation also ensures that the number of mesh points per wavelength also remains constant since the refractive index increases and thus the local wavelength decreases in precisely those areas where the mesh is denser. Finally, since this expansion is conformal the overall transformation remains conformal making it easy to transform the end results back into real space.

3. Results

In the previous section we showed how a transformational optics approach converts non-rectangular domains to rectangular domains at the expense of more complicated material parameters. Here we show that this approach is more efficient and accurate when using the standard FDTD method. We start with the example shown Fig. 1(a) where we consider the boundaries to be perfect electrical conductors (PEC) and so it is a non-uniform 2D waveguide. Of interest to us is the amount of light reflected in the TE^1 mode for a pulsed excitation of the same mode. As the field distributions for the different modes are orthogonal, we can define the reflection coefficient for the nth mode, $S_{1n,}$ as

$$S_{1n} = \frac{F\{\int (E^{\perp}_{total} - E^{\perp}_{incident}) E^{\perp}_{n} dl\}}{F\{\int |E^{\perp}_{incident}|^2 dl\}} \tag{14}$$

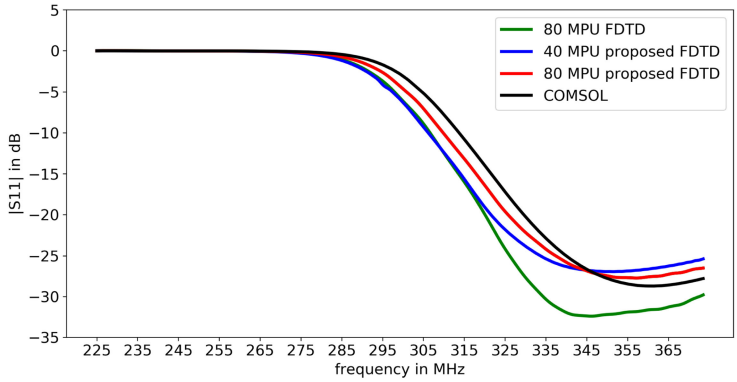

Fig. 6. Calculated S_{11} for the waveguide shown in Fig. 1(a).

TABLE 1
MPU, Total Number of Meshes and the Run Time for Classical FDTD and Our Proposed Method

Method	*MPU*	*Total number of meshes*	*error*	*Run time*
Proposed FDTD	40	28028	-20.61dB	30s
Classical FDTD	80	94416	-20.92dB	139s

in which, $E^{\perp}_{total}$, $E^{\perp}_{incident}$ and $E^{\perp}_{n}$ are the perpendicular total, incident and nth mode electric field and F is the symbol of the Fourier transformation. We compare our calculated value of S_{11} against both the results of an FDTD simulation in real space and the results of a FEM method using the commercial software COMSOL and our results are illustrated in Fig. 6 across a range of frequencies. Note that we have assumed that the FEM simulation is correct since a triangular mesh can be readily adapted to arbitrary geometries and situations. However, the downside is that it takes an exceedingly long time to run and thus it is hard to use for numerical optimization. We can see that our proposed method is more accurate than conventional FDTD even when using half the number of meshing cells per unit length. We quantify the error as being the log of the integrated frequency dependent difference between the FEM solution and our current FDTD method i.e.:

$$error = 10\log\left(\frac{\int_{f_1}^{f_2}\left(S_{11_{comsol}} - S_{11}\right)^2 df}{f_2 - f_1}\right) \tag{15}$$

in which the f_2 and f_2 are maximum and minimum frequencies of simulation. The simulation times for both conventional FDTD with 80 mesh points per unit length and our more accurate proposed method for 40 mesh points per unit length are given in Table 1. Note that even with 40 MPU the improved method is more accurate at higher frequencies and substantially quicker that the standard method with 80 MPU. Although we have only discussed 2D simulations in this work, similar improved scalings should hold in 3D where we would expect a much greater time saving since the time goes as the cube of the MPU.

Our second example is the waveguide with the boundary discontinuity previously shown in Fig. 5(a). As before we exit the TE^1 mode at the left-hand boundary and measure the amount of reflected light in the same mode. The calculated S_{11} coefficients for the conventional FDTD algorithm, COMSOL and our proposed method for different MPU and across a wide frequency range are illustrated in Fig. 7(a) and (b). These figures clearly show that our proposed method

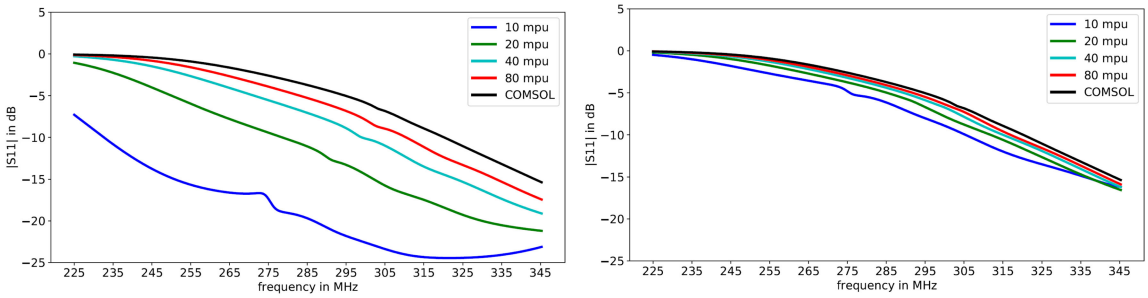

Fig. 7. Calculated S_{11} for the waveguide depicted in Fig. 5(a) using (a) classical FDTD and (b) proposed method.

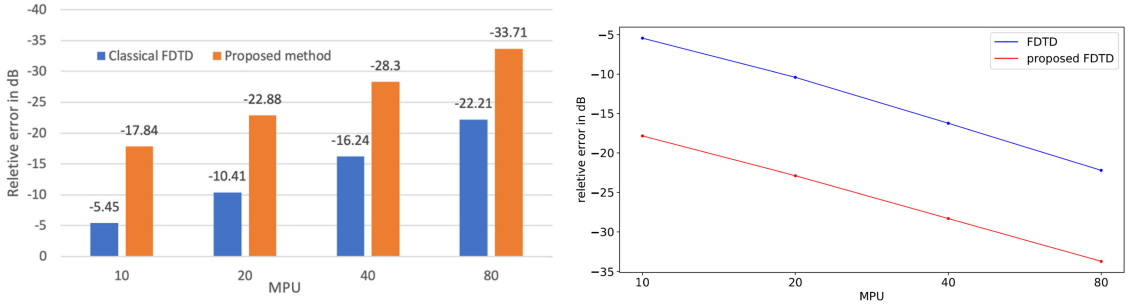

Fig. 8. Numerical error for classical FDTD and the proposed method.

TABLE 2
Total Number of Meshes, Error and the Run Time for Our Proposed Method

MPU	*Total number of meshes*	*Error*	*Run time*
10	1736	-17.84dB	.46s
20	5856	-22.88dB	1.75s
40	21296	-28.30dB	9.15s
80	80976	-33.71dB	74.88s

converges more rapidly in comparison with the conventional FDTD algorithm. The reduction in error [calculated using Eq. (15)] as a function of mesh size for both the conventional FDTD and the proposed method is shown in Fig. 8.

In this example our proposed method is more accurate than the conventional FDTD algorithm even with 16 times few points (corresponding to a 4-fold reduction in MPU) and so substantial speedups can be observed. In this case there are two reasons for the improved accuracy. The first is the use of discrete meshing sections to avoid material singularities as discussed in Section 2.1. Secondly, we have used a suitable rotation matrix that allows the mesh to smoothly follow the boundary with no staircase errors. The detail about the run time, total number of meshing cells and the amount of errors are shown in Table 2 and 3 for the proposed method and classical FDTD,

TABLE 3
Total Number of Meshes, Error and the Run Time for Classical FDTD

MPU	*Total number of meshes*	*Error*	*Run time*
10	1456	-5.45dB	.22s
20	4896	-10.41dB	.76s
40	17776	-16.24dB	3.69s
80	67536	-22.21dB	30.80s

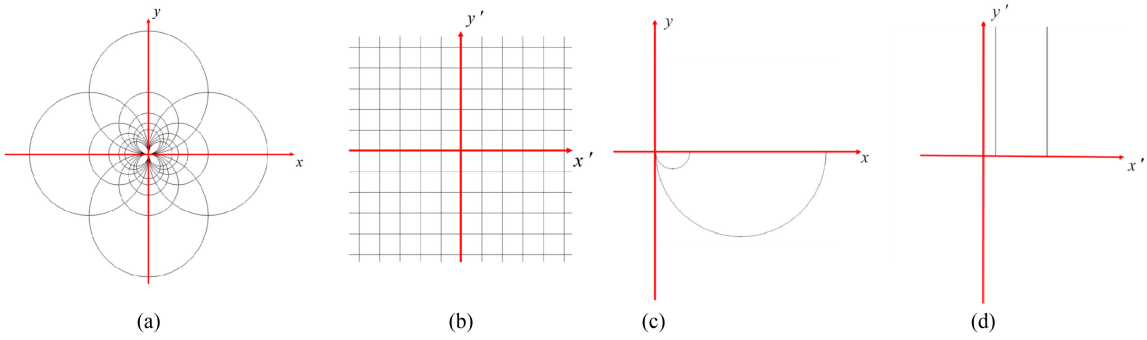

Fig. 9. (a) and (b) physical and virtual space grid based on 1/Z conformal transformation. (c) and (d) physical and virtual space scenarios based on the same transformation.

respectively. For example, when we target a numerical error less than -22 dB, our method runs more than 17 times faster than classical FDTD.

The last example is a metal insulator metal plasmonic structure for SERS shown in Fig. 9(c). This structure has previously been investigated and fabricated in [11], [12] and [23]. In Ref [23] it was shown that although this structure has a dimension around 1 micron it enhanced the Raman signal by more than a factor of 10^6. We have chosen to simulate this geometry since it shows the limitation of the approach developed in Ref [19] as the structure's dimensions are greater than 200 nm. This structure also illustrates the issues involved when using a conformal transformation. First consider the conformal transformation given by $f(z) = 1/z$ where z is a complex number. This mapping and effect of it on the coordinate grids in physical and virtual space are illustrated in Fig. 9(a) and (b), respectively. Note that it converts circles touching the origin into straight lines and maps the origin itself to infinity. Thus, we need to avoid the use of singular transformations as discussed in Section 2.2. The geometry that we wish to model is shown in Fig. 9(c), which comprises two circles of differing radius that touch at the origin. This is then gets mapped to the infinite rectangle shown in Fig. 9(d). This is in fact precisely half of the structure used in Ref. 23 and so we can simulate the complete structure using symmetry and the appropriate boundary conditions. However, modelling half the structure allows for better visualization and so that is the approach we have adopted. For this example, the boundaries and all the area beyond them are chosen to be gold.

The simulation results for the E_x field distribution for proposed FDTD and COMSOL are presented in Fig. 10(a) and (b). All the length units in these figures are normalized to 933 nm which is the biggest dimension of this structure. The simulation has been done for monochrome light with wavelength of 700 nm and the gold permittivity has been chosen form Johnson and Christy data [29] which is $-16.486-1.0643$i at this frequency. The meshing scheme in physical space is shown in Fig. 10(c) which gets converted into a uniform grid. As a comparison we have calculated the E_x

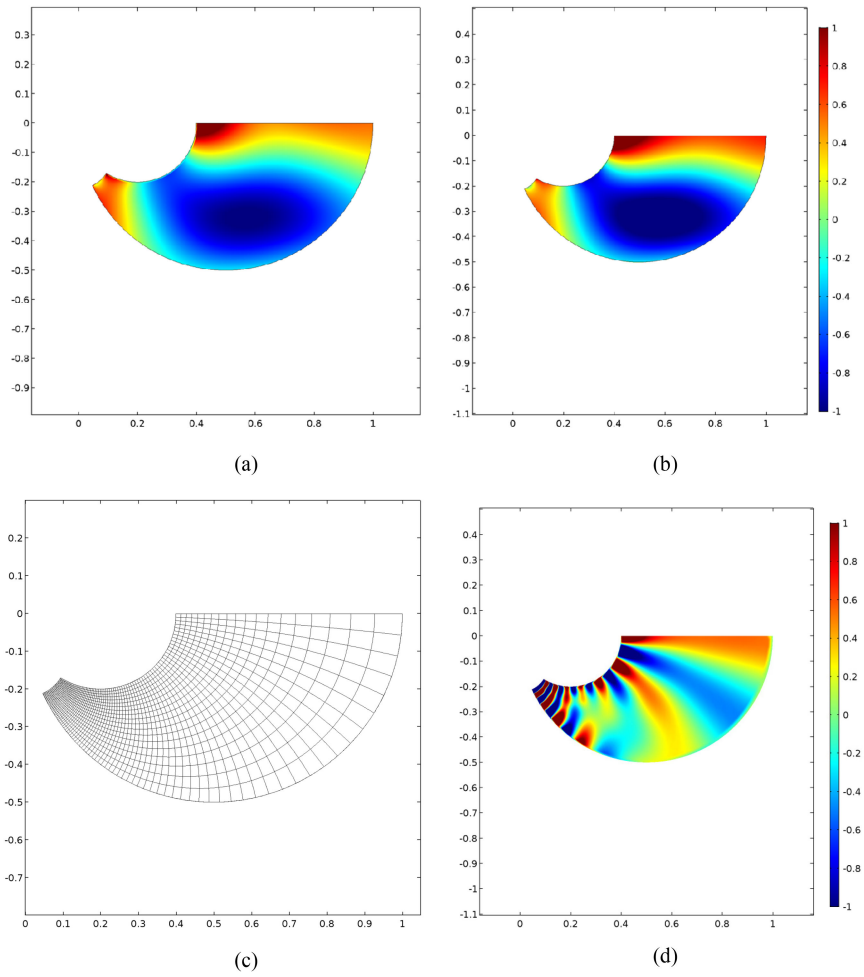

Fig. 10. (a) and (b) E_x field distribution using the proposed FDTD and FEM method. (c) meshing schematic in physical space. (d) E_x field distribution using the method presented in [19].

field distribution using the semi-analytical methodology presented in [19] and the results are shown in Fig. 10(d). As we can see, the methodology in [19] (or similar semi-analytic approaches) cannot be applied to this structure due to the range of feature sizes compared to the incident wavelength. This shows that our numerical approach will succeed even when analytical results fail.

In this case we also checked that our algorithm did not suffer from the onset of "late-time instabilities" such as those that afflict other FDTD approaches Refs. [14], [15]. We ran the SERS simulation over 1 million time steps corresponding to more than 2000 round trips through the structure and no numerical instabilities has been observed. However, some other weaknesses of numerical analysis such as inconsideration of lossy medium to find the fundamental mode's equivalent refractive index [30], [31] should be studied and is suggested as the extension of the present work.

4. Conclusion

A novel FDTD method based on transformation optics was proposed and implemented. Compared to previous transformation optics based approaches our method avoids singularities and zeros in the transformed materials. We further showed how unwanted material dispersion can be eliminated

through a second transformation. We used this method in investigate different structures for SERS based on MIM as well as different waveguide geometries. This method was found to be at faster and more accurate than the standard FDTD algorithm and previously introduced semi-analytically methods without facing additional problems such as late-time instabilities material dispersion. Our proposed method can improve the accuracy and functionality of FDTD in many applications areas dealing with complex boundaries such as waveguide and scattering problems across a wide range of frequencies.

Acknowledgment

The work presented in this paper was sponsored by the Dodd-Walls Centre for Photonic and Quantum Technologies, and The Goodfellow Fund for Support of Urological Research, New Zealand.

References

[1] J. Singh, S. Juneja, A. Ghosal, and A. Ghosal, "Energy harvesting: Role of plasmonic nanocomposites for energy efficient devices," in *Proc. Integr. Green Chemistry Sustain. Eng.*, 2019, pp. 81–112.
[2] I. Fabijanić *et al.*, "Plasmonic nanoparticles and Island films for solar energy harvesting: A comparative study of Cu, Al, Ag and Au performance," *Coatings*, vol. 9, no. 6, p. 382, 2019.
[3] A. A. Popov *et al.*, "Laser-synthesized TiN nanoparticles as promising plasmonic alternative for biomedical applications," *Scientific reports*, vol. 9, no. 1, 2019, Art. no. 1194.
[4] Y. Huang, P. Huang, and J. Lin, "Plasmonic gold nanovesicles for biomedical applications," *Small Methods*, vol. 3, no. 3, 2019, Art. no. 1800394.
[5] G. Marino *et al.*, "Second-harmonic generation from hyperbolic plasmonic nanorod metamaterial slab," *Laser Photon. Rev.*, vol. 12, no. 2, 2018, Art. no. 1700189.
[6] J. Yu, S. Park, I. Hwang, D. Kim, J. Y. Jung, and J. Lee, "Third-harmonic generation from plasmonic metasurfaces coupled to intersubband transitions," *Adv. Opt. Mater.*, vol. 7, no. 9, 2019, Art. no. 1801510.
[7] P. L. Stiles, J. A. Dieringer, N. C. Shah, and R. P. Van Duyne, "Surface-enhanced Raman spectroscopy," *Annu. Rev. Anal. Chem.*, vol. 1, pp. 601–626, 2008.
[8] F. J. García-Vidal and J. B. Pendry, "Collective theory for surface enhanced Raman scattering," *Physical Rev. Lett.*, vol. 77, no. 6, 1996, Art. no. 1163.
[9] Y. Luo, A. Aubry, and J. B. Pendry, "Electromagnetic contribution to surface-enhanced Raman scattering from rough metal surfaces: A transformation optics approach," *Physical Rev. B*, vol. 83, no. 15, 2011, Art. no. 155422.
[10] T. Fu *et al.*, "Numerical investigating plasmon sensitivity and SERS enhancement of individual TiN nanosphere multimers," *Nanotechnology* , vol. 31, 2019, Art. no. 135210.
[11] M. Kazemzadeh, N. Broderick, W. Xu, and K. Z. Shoshtari, "Design and optimization of broadband and transparent SERS based on transformation optics," *SPIE Micro+ Nano Mater., Devices, Appl., Int. Soc. Opt. Photon.*, vol. 11201, 2019, Art. no. 112011L.
[12] P. Mao *et al.*, "Broadband single molecule SERS detection designed by warped optical spaces," *Nature Commun.*, vol. 9, no. 1, 2018, Art. no. 5428.
[13] R. Chen, L. Kuang, Z. Zheng, and Q. H. Liu, "A novel transformation optics-based FDTD algorithm for fast electromagnetic analysis of small structures in a large scope," *IEEE Access*, vol. 7, pp. 124750–124758, 2019.
[14] A. T. Hayder, J. P. Bérenger, and F. Costen, "Singularity problem with the one-sheet huygens subgridding method," *IEEE Trans. Electromagn. Compat.*, vol. 59, no. 3, pp. 992–995, Jun. 2017.
[15] J. P. Bérenger, "The Huygens subgridding for the numerical solution of the Maxwell equations," *J. Comput. Phys.*, vol. 230, no. 14, pp. 5635–5659, 2011.
[16] Y. Luo, R. Zhao, A. I. Fernandez-Dominguez, S. A. Maier, and J. B. Pendry, "Harvesting light with transformation optics," *Sci. China Inf. Sci.*, vol. 56, no. 12, pp. 1–13, 2013.
[17] Y. Luo, A. Aubry, and J. B. Pendry, "Electromagnetic contribution to surface-enhanced Raman scattering from rough metal surfaces: A transformation optics approach," *Physical Rev. B*, vol. 83, no. 15, 2011, Art. no. 155422.
[18] Y. Luo, D. Y. Lei, S. A. Maier, and J. B. Pendry, "Broadband light harvesting nanostructures robust to edge bluntness," *Physical Rev. Lett.*, vol. 108, no. 2, 2012, Art. no. 023901.
[19] J. B. Pendry, A. Aubry, D. R. Smith, and S. A. Maier, "Transformation optics and subwavelength control of light," *Sci.*, vol. 337, no. 6094, pp. 549–552, 2012.
[20] A. I. Fernández-Domínguez, S. A. Maier, and J. B. Pendry, "Transformation optics description of touching metal nanospheres," *Physical Rev. B*, vol. 85, no. 16, 2012, Art. no. 165148.
[21] J. B. Pendry, D. Schurig, and D. R. Smith, "Controlling electromagnetic fields," *Sci.*, vol. 312, no. 5781, pp. 1780–1782, 2006.
[22] L. Xu, and H. Chen, "Conformal transformation optics," *Nature Photon.*, vol. 9, 1, pp. 15–23, 2015.
[23] M. Focsan *et al.*, "Flexible and tunable 3D gold nanocups platform as plasmonic biosensor for specific dual LSPR-SERS immuno-detection," *Scientific Rep.*, vol. 7, no. 1, 2017, Art. no. 14240.
[24] J. Liu, M. Brio, and J. V. Moloney, "Transformation optics based local mesh refinement for solving Maxwell's equations," *J. Comput. Phys.*, vol. 258, pp. 359–370, 2014.

[25] A. J. Strong, "Transformation optics based finite-difference time-domain simulation of superscattering," Ph.D. dissertation, Delaware State Univ., Dover, OH, USA, 2019. [Online]. Available: http://hdl.handle.net/20.500.12090/387
[26] R. Chen, L. Kuang, P. Ren, and Q. H. Liu, "Modified transformation optics based FDTD for local mesh refinement, in *Proc. Progr. Electromagn. Res. Symp. (PIERS-Toyama)*, Toyama, Japan, 2018, pp. 1138–1140, doi: 10.23919/PIERS.2018.8597914.
[27] R. Chen, L. Kuang, Z. Zheng, and Q. H. Liu, "Transformation optics-based finite difference time domain algorithm for scattering from object with thin dielectric coating," *IEEE Access*, vol. 7, pp. 150060–150071, 2019.
[28] M. R. Kazemzadeh, and A. Alighanbari, "3-D implementation of transformation optics using a tetrahedron-based meshing technique and homogeneous materials," *IEEE Trans. Antennas Propag.*, vol. 65, no. 7, pp. 3549–3559, Jul. 2017.
[29] P. B. Johnson, & R. W. Christy, "Optical constants of the noble metals," *Physical Rev. B*, vol. 6, no. 12, 1972, Art. no. 4370.
[30] B. A. Rahman, and J. B. Davies, "Penalty function improvement of waveguide solution by finite elements," *IEEE Trans. Microw. Theory Techn.*, vol. 32, no. 8, pp. 922–928, Aug. 1984.
[31] R. Bhattacharjee, N. T. Kejalakshmy, and B. A. Rahman, "Design and optimization of an Al doped ZnO in Si-slot for gas sensing," *IEEE Photon. J.*, vol. 10, no. 4, Aug. 2018, Art no. 6803110.